Influence of the Meridional Overturning Circulation on Tropical Atlantic Climate and Variability

Reindert Haarsma[1], Edmo Campos[2], Wilco Hazeleger[1], Camiel Severijns[1]

[1]Royal Netherlands Meteorological Institute (KNMI), Netherlands
[2]Oceanographic Institute, University of São Paulo (IOUSP), Brazil

Corresponding author:
Reindert Haarsma
Royal Netherlands Meteorological Institute (KNMI)
P.O. Box 201
3730 AE De Bilt
The Netherlands
haarsma@knmi.nl

Submitted to Journal of Climate
Revised version

ABSTRACT

The influence of the meridional overturning circulation on tropical Atlantic climate and variability has been investigated using the atmosphere-ocean coupled model Speedy-MICOM. In the ocean model MICOM the strength of the meridional overturning cell can be regulated by specifying the lateral boundary conditions. In case of a collapse of the basin-wide meridional overturning cell the SST response in the Atlantic is characterized by a dipole with a cooling in the North Atlantic and a warming in the tropical and South Atlantic. The cooling in the North Atlantic is due to the decrease in the strength of the western boundary currents which reduces the northward advection of heat. The warming in the tropical Atlantic is caused by a reduced ventilation of water originating from the South Atlantic. This effect is most prominent in the eastern tropical Atlantic during boreal summer when then the mixed layer attains its minimum depth. As a consequence the seasonal cycle as well as the interannual variability in SST are reduced. The characteristics of the cold tongue mode are changed: The variability in the eastern equatorial region is strongly reduced and the largest variability is now in the Benguela region. Due to the deepening of the equatorial thermocline, variations in the thermocline depth in the eastern tropical Atlantic no longer significantly affect the mixed layer temperature. The gradient mode remains unaltered. The warming of the tropical Atlantic enhances and shifts the Hadley circulation. Together with the cooling in the North Atlantic, this increases the strength of the subtropical jet and the baroclincity over the North Atlantic.

1. Introduction

Recent modeling studies with coupled climate models suggest that major changes in the strength of the meridional overturning circulation (MOC) significantly affect the atmospheric and oceanic circulation on a global scale. Vellinga and Wood (2002) and Dahl et al. (2005) found that a weakened MOC results in a dipole response over the Atlantic, with a cooling in the North Atlantic and a warming in the tropical and South Atlantic. Similar results were found by Zhang and Delworth (2005), together with a significant El-Niño like response in the tropical Pacific and a southward shift of the intertropical convergence zone (ITCZ) over the Atlantic and Pacific. A recent intercomparison of 14 models ranging from earth system models of intermediate complexity to fully coupled atmosphere-ocean circulation models by Stouffer et al. (2006) revealed the robustness of certain aspects of the response by a collapse of the MOC, like the dipole response in sea surface temperature (SST) and the southward shift of the ITCZ. These results appear to be corroborated by paleo-records (Stott et. al. 2002; Peterson et al. 2000).

Because the seasonal cycle and interannual variability are strongly linked to the climatological mean state, it is expected that they also will be affected by a weakened MOC. The changes in the seasonal cycle and interannual variability might be profound and exceed the changes in the mean state. The interannual variability in the tropical Atlantic is dominated by two modes of variability: the cold tongue mode and the gradient mode (Hastenrath 1978; Ruiz-Barradas et al. 2000). The physical mechanism of the cold tongue mode appears to be similar to the El-Niño mode in the Pacific ocean: It is also the result of a "Bjerknes-Feedback", with a crucial role for the ocean dynamics (Zebiak 1993; Keenlyside and Latif 2007; Carton and Huang 1994). The Atlantic cold tongue mode is tied to the

seasonal cycle and attains its maximum amplitude during the boreal summer, when the west African monsoon drives shoaling of the mixed layer in the eastern tropical Atlantic. The gradient mode is driven by changes in the trade winds which are related to variability in the North Atlantic Oscillation (NAO) and amplified by the wind evaporation (WES) feedback (Czaja et al. 2002; Breugem et al. 2007a; Xie 1999). It is strongly connected to the seasonal cycle of the ITCZ. These modes of variability have a large impact on rainfall in west Africa and north-east Brazil. A comprehensive overview of tropical Atlantic variability has been given by Xie and Carton (2004).

Here we analyze the response of tropical Atlantic climate and variability in a global atmosphere model coupled to an ocean model of the Atlantic basin. The model Speedy-MICOM simulates the tropical Atlantic variability realistically (Hazeleger and Haarsma 2005) (HH2005). By perturbing the northern and southern lateral boundary conditions in the ocean we can mimic an MOC collapse. The results will be discussed in relation to past changes in MOC and ITCZ and to future changes when the MOC is expected to decrease (Gregory et al 2005). Since state-of-the-art coupled models do not simulate realistic tropical Atlantic variability (Breugem et al. 2007b), this regionally coupled model can give insight on the response of the tropical Atlantic variability to changes in the future.

In section 2 we will describe the model and the set-up of the experiments. The results are presented in section 3, followed by a discussion and conclusions in section 4.

2. Speedy-MICOM

The coupled Speedy-MICOM model (Hazeleger et al. 2003) is the same as used in HH2005 and will only briefly described here. It consists of an atmospheric primitive equation model (Speedy) with a vertical resolution of seven layers and a triangular spectral truncation at total wavenumber 30 (T30). The model has simplified physics which makes it computationally inexpensive. A five layer version is

described in detail by Molteni (2003). The ocean component consists of the Miami Isopycnic Coordinate Ocean Model (MICOM version 2.7, Bleck et al. 1992). The model uses potential density as vertical coordinate. It is configurated at 22 layers and has a horizontal resolution of 1 degree. The MICOM model is configurated for the Atlantic basin from 45^{o} S to 60^{o} N. Restoring boundary conditions of the thermodynamic properties are applied at the northern and southern lateral boundaries. Outside the Atlantic basin and over land climatological surface temperature is prescribed. In HH2005 it is shown that for present conditions Speedy-MICOM reproduces well the tropical Atlantic climatology including the east-west tilt of the thermocline along the equator. For most of the tropical Atlantic the error in SST is less than 2^{o} C. As a result Speedy-MICOM simulates realistically the tropical Atlantic variability including the gradient mode and the cold tongue mode. Figure 1 repeats from HH2005 the structures of the cold tongue mode and the gradient mode, computed by a rotated empirical orthogonal function (REOF) analysis. They compare well with the modes as analyzed by Ruiz-Barradas et al. (2000). The main deficiency of the cold tongue mode is that is located about 10 degrees too far to the east. The dynamics of these modes appears to be similar to what is known from observations. The main heat balance for the cold tongue mode is forcing by vertical entrainment and damping by latent heat flux (Hazeleger 2007 in preparation). The atmospheric response includes a "Bjerknes" feedback as indicated by the wind stress in Fig. 1a. The gradient mode is forced by latent heat flux resulting from variations in the trade winds. It is amplified by the WES feedback (Breugem et al. 2007a).

With Speedy-MICOM we have performed two runs: A control run (CONTROL) representing present day conditions and a run in which the MOC is strongly reduced (NO-MOC). For the control run the lateral boundaries are taken from Levitus et al. (1998). The control run is the same as discussed in HH2005 and in Haarsma and Hazeleger (2007) (HH2007). For the NO-MOC run the lateral boundaries are obtained from a global MICOM run with the same resolution and parameterizations that was forced with CORE surface fluxes (Large and Yeager 2004). Despite realistic atmospheric forcing this run is

characterized by a collapsed MOC due to insufficient deep-water formation in the North Atlantic. Most of the ocean-ice models forced by the CORE fluxes show a MOC collapse, which is probably due to too high freshwater fluxes in the Arctic (Griffies, Personal communication). Although this run suffers from the inability to simulate a MOC in accordance with the observations, it serves our goal to provide boundaries for a run with a reduced MOC. Outside the Atlantic MICOM basin the SST are prescribed using present day climatology. Although a collapse of the MOC will have a global impact affecting the SSTs outside the Atlantic, this set-up allows us to investigate the local processes over the Atlantic.

The boundary conditions for temperature and salinity for the CONTROL and NO-MOC run are shown in Fig. 2. Compared to the CONTROL run, for the NO-MOC run at the northern boundary there is a cooling at all depths ranging from about 1 ^{o}C at the surface to about 2 ^{o}C in the deep ocean. The southern boundary shows a small warming of 0.5 ^{o}C at the surface and a similar cooling of 2 ^{o}C in the deep ocean. A rather uniform freshening in the order of 0.2 PSU occurs at the northern boundary at all depths, whereas the southern boundary shows a freshening at the mixed layer, more saline conditions below the mixed layer, and freshening again below 1500 m. Figure 2c shows that these changes in temperature and salinity result for the NO-MOC boundaries in a difference in density between the northern and southern boundary, which is close to zero over almost the entire column (dashed line). It is therefore expected that these new boundaries will not generate a significant MOC circulation, in contrast to the boundaries in the CONTROL run which induce denser water in the North Atlantic compared to the South Atlantic (solid line). The cooling and freshening at the northern boundary is consistent with the decrease in deep water formation in the northern seas. The more saline conditions between the mixed layer and 1500 m at the southern border reflect the reduction of the inflow of Antarctic intermediate water (AAIW) and Sub Antarctic mode water (SAMW). Weijer et al. (1999) estimated the heat and salt fluxes at 30^{o} S and their contributions to the overturning circulation. These profiles are characterized by a positive heat flux and a negative salt flux in the upper ocean (their Figs.

1 and 4). The cooler and more saline conditions of the subsurface waters at the southern border in case of no overturning circulation therefore agree with Weijer et al. (1999).

Starting from the control state the model with the new boundaries was run for 100 years. In the following the results averaged over the last 45 years are shown. For this period the atmosphere and the upper 1000 m of the ocean are in equilibrium. The deep ocean still shows a trend of about 0.3 ^{o}C over these last 45 years. This is however much less than the differences between the CONTROL and the NO-MOC run as will be shown below.

3. Results

The change in the lateral boundaries strongly modifies the ocean circulation. Fig 3 shows the response in the sea surface temperature SST and seas surface salinity (SSS) distribution. The changes in SST reveal a dipole pattern with a cooling in the North Atlantic and warming in the tropical and South Atlantic (Fig. 3a). This pattern is similar to that obtained in other modeling studies (Vellinga and Wood 2002; Dahl et al. 2005; Zhang and Delworth 2005). Strong cooling of about 10 ^{o}C occurs in the north western Atlantic, whereas the tropical Atlantic warms about 0.5-1.5 ^{o}C. However, despite these similarities also notable differences exist. The simulated cooling over the tropical Atlantic is weaker than simulated by state-of-the-art general circulation models (GCMs) (i.e. Zhang and Delworth 2005). In addition the warming in eastern tropical north Atlantic is not simulated in those GCMs. These differences might be due to the simplified atmospheric physics used by the model. Yang and Liu (2005) have shown that the atmospheric circulation induced by extra-tropical cooling can contribute to two thirds of the tropical SST dipole anomalies. The changes in SSS (Fig. 3b) show a similar pattern as the SST changes, with a strong freshening of about 2 PSU in the northern part of the North Atlantic and more saline waters in the tropical and south Atlantic. In addition in the North Atlantic a subtropical band of more saline waters is seen. The changes in SST will change the atmospheric circulation. These

changes in the atmospheric circulation will then feed back on the ocean circulation due to changes in wind stress and heat and fresh water fluxes. In order to facilitate the analysis of the coupled response, we will first discuss in section 3.1 the atmospheric response to the changes in SST and next in section 3.2 the changes in the ocean circulation caused by the changed lateral boundary conditions and changes in the atmospheric circulation. Finally in section 3.3 we will discuss the implications for the tropical Atlantic variability.

3.1 Atmosphere response

The warming of the tropical Atlantic enhances the Hadley circulation over the Atlantic as shown in Fig. 4. The increase of the Hadley circulation is most pronounced during boreal summer (Fig. 4b) when the increase of tropical SSTs is largest. During this season the increase in ω is about 30%. In addition to the strengthening there is a southward shift of a few degrees during the boreal summer when the Hadley circulation is at its northern most position. The change in strength of the Hadley circulation is less during DJF because the changes in SST are less as will be discussed below (see Fig. 9b). For this season Speedy simulates a northward shift of the Hadley circulation. This might however be an artifact of Speedy because it simulates an ITCZ that is located south of the equator during this season. This implies that increased equatorial SSTs will shift the ITCZ northward. In observations the ITCZ always remains north of the equator. The rainfall changes are shown in Fig. 5, revealing the shift and increase in intensity of the ITCZ. The largest changes in rainfall occur during JJA and are in the order of 4 mm/day. During this season the ITCZ is shifted southward, whereas it is shifted northward during DJF

Figure 3a shows for the annual mean the increase in the trade winds due to the increase of the Hadley circulation. The increase is largest for the north-eastern trade winds. This is due to a southward shift of the Hadley circulation. The increase in the north-eastern trade winds induces a WES feedback

(Chang et al. 1997) that contributes to the cooling over the subtropical North Atlantic shown in Fig. 3a. Close to the African continent the monsoon winds decrease due to the decrease in the land-sea temperature contrast, resulting from the temperature rise in the eastern tropical Atlantic. In the North Atlantic an anomalous anti-cyclonic circulation is seen. This is caused by the anomalous cold SSTs in the north western Atlantic, which generate a baroclinic response over the anomaly with a low level anti-cyclonic circulation.

In HH2007 it was shown that during the warm phase of the cold tongue mode the jet over the North Atlantic is enhanced and shifted equator ward. The mechanism outlined in HH2007 follows the ideas of Lee and Kim (2003) and Son and Lee (2005). The local increase in the Hadley circulation, forced by the warm SSTs, enhances the subtropical jet. The resulting increase in the vertical shear of the zonal wind increases the baroclinicity over the southern part of the North Atlantic. This induces a southward shift of the jet. The NO-MOC run induces a large scale warming of the tropical Atlantic, suggesting a similar response. In addition the NO-MOC run shows a strong cooling in the northern part of the North Atlantic. According to Son and Lee (2005) this broadens the extra-tropical baroclinic zone and enhances the southward shift over the North Atlantic. Figure 6 reveals that indeed the jet over the Atlantic is enhanced and shifted equator ward. Further analysis revealed that similar as in HH2007 this is related to an increase and equatorward shift of the baroclinicity. Over the equator the enhanced warming of the eastern tropical Atlantic affects the Walker circulation inducing easterlies.

3.2 Ocean Response

To understand the origins of the SST changes in the mixed layer we analyzed the heat budget. Figure 7a shows the changes in the net surface heat flux (downward is positive). For most regions the sign of the SST change is of opposite sign of the net surface heat flux from which we infer that the

atmosphere opposes the changes in the mixed layer temperature and that they are generated by changes in ocean heat transport. Analysis of the ocean heat transport reveals that the strong cooling in the north-western Atlantic is dominated by changes in horizontal ocean heat transport caused by the reduction of the western boundary current (not shown). For the tropical Atlantic the main contribution to the warming in the NO-MOC experiment is the reduction of the oceanic cooling due to vertical entrainment (Fig. 7b). This results in a strong warming of the mixed layer along the eastern part of the equator and in the upwelling zones along the eastern coast. North of the warming in the tropical Atlantic there is small band of negative SST anomalies in the south-east north-west direction at 20º N. Figure 7a reveals a warming by the atmosphere, indicating that the cooling is caused by the ocean heat transport. Further analysis indicates that for this band the most important contribution comes from the horizontal south-westerly advection of anomalous cold water by the mean currents, although close to the North African coast also anomalous vertical advection appears to be important. Although the increase in wind speed due to the increase of the north-eastern trade winds induces a cooling this is not seen in the change of the net surface heat flux. From this we infer that this effect is of minor importance. The atmospheric circulation might play an important role during the initial stage of the MOC collapse by transporting the cooling over the region of deep water formation area equator ward. This is, however, outside the scope of this study, which deals with the final equilibrium state.

North of the equator in the tropics, the increase in SSS, which is caused by the collapse of the MOC, is counteracted by the enhanced precipitation resulting from the increase in the Hadley circulation. This causes the negative SSS anomalies between 0-5° N in Fig. 3b. The increase in North Atlantic subtropical SSS is due to the reduction of the western boundary current, which increases the residence time of surface waters in the subtropics. The strong evaporation in this region increases the SSS. A south-east north-west band at 20º N with fresh water is seen, similar in structure as observed for the SST, which is caused by the advection of anomalous cold and fresh water by the mean currents as

discussed above.

As described, the dominant changes in SST and SSS are forced by changes in the ocean circulation, which can be described in terms of changes in the meridional overturning circulation (MOC) (Fig.8). The MOC of the CONTROL experiment (Fig. 8a) is about 20 Sv. The upwelling in the equatorial region is about 10 Sv, of which 2 Sv is due to the northern subtropical cell (STC). The meridional heat transport is about 1 Pw (Fig. 8c). The values for the meridional overturning and heat transport are approximately in agreement with the observations (Trenberth and Caron 2001; Ganachaud and Wunsch 2003). The main deficiency is the absence of a clear zonal mean STC in the South Atlantic (Hazeleger and Drijfhout 2006). In the NO-MOC experiment the basin-wide MOC is completely collapsed due to the vanishing of the meridional density difference between the lateral boundaries and the circulation is now dominated by two STCs of 2 and 6 Sv in the South and North Atlantic respectively as shown in Fig. 8b. The increase in the STCs is due to the increase in the trade winds caused by the enhancement of the Hadley circulation. The stronger increase of the north Atlantic STC is in accordance with the enhanced increase of the north easterly trades. The increase in the trade winds also results in a 10% stronger equatorial under current (EUC), which extends further to the east (not shown). The meridional heat transport is strongly reduced to from 1 Pw to 0.3 Pw (Fig. 8c), implying a northward heat transport by the basin-wide MOC of about 0.7 Pw. This compares favorably with the 0.86 Pw of Hazeleger and Drijfhout (2006).

This large change in the Atlantic circulation not only affects the SST and SSS but the temperature and salinity distribution in the entire ocean. Figure 9 shows that in the tropical Atlantic the largest warming (about 5 ^{o}C) occurs in the thermocline. The depth of the thermocline as indicated by the 20 °C isotherm increases by about 25 m. A large warming is also seen in the North Brazil under Current (NBUC). The mixed layer warms about 0.5-1.5 ^{o}C. Below the thermocline the tropical ocean is a few degrees cooler. The cooling of the deep ocean is to be expected due to the reduction in

temperature for the deep ocean in the northern and southern boundaries for the NO-MOC run compared to those for the CONTROL run and the more stable stratification (Fig. 2). The collapse of the basin-wide MOC reduces the upwelling of cold water in the equatorial Atlantic (Fig. 8b). The circulation is now dominated by the two STCs and the water that ventilates in the equatorial mixed layer is predominantly originating from the subtropics. The reduced upwelling ($w'\nabla\mathbf{T}$) and warmer source water (i.e. $\mathbf{w}\nabla T'$) both contribute to the rise of the upper ocean temperature. The atmospheric response induces an enhanced Ekman upwelling in the eastern Atlantic just north of the equator (not shown). The enhanced Ekman upwelling explains that the rise in SST north of the equator is reduced and that the largest increase in SST is just south of the equator (Fig. 3a). The impact of the enhanced Ekman upwelling is also seen in the mixed layer thickness, which is displayed in Fig. 10. This figure reveals that the deepening of the tropical eastern Atlantic is restricted to the area south of the equator, and shows no deepening in the eastern tropical Atlantic just north of the Equator. The strongest deepening occurs in the upwelling regions at the African coast. The very strong shoaling of the mixed layer seen in the north-west Atlantic is induced by the lateral boundary conditions and reflects that the boundaries of the NO-MOC run are taken from a state of no deep-water formation. The reduction of the mixed layer depth in the cool south-west north-east band in the subtropical North Atlantic (Fig. 3a) underscores the conclusion made before, that the cooling by enhanced north-eastern trade winds only plays a minor role in generating this cool SST band.

The entrainment in the eastern tropical Atlantic and its reduction display a semi-annual cycle as shown in Fig. 11a. The entrainment and its reduction are largest during the boreal summer (JJA). A secondary maximum in entrainment occurs during winter (DJF). During the boreal summer the mixed layer depth attains its minimal value due to the strong upwelling caused by the west African monsoon. Changes in vertical entrainment will have then the largest impact on the heat budget of the mixed layer due to its reduced heat capacity. During this period the increase in SST, which is then at its lowest

value, is largest in the order of 2 ^{o}C as shown in Fig. 11b. The change in SST during winter is small. During this period the reduction in entrainment is preceded by an increase at the eastern boundary (Fig. 11a).

3.3 Implications for tropical Atlantic variability

The changes in the mean state and the seasonal cycle affect the interannual variability in the tropical Atlantic. The standard deviation of the monthly mean SST anomalies (Fig. 12) reveals large changes with respect to the CONTROL simulation. The largest changes are in the region of the cold tongue mode where the standard deviation is reduced from about 0.7 to 0.4 ^{o}C, in the region of the gradient mode it is reduced from 0.6 to 0.5 ^{o}C. These changes in the standard deviation reflect the changes in the modes of variability in the tropical Atlantic.

3.3.1 Cold tongue mode

The REOF analysis of monthly mean anomalous SST shown in Fig. 13a reveals indeed that the cold tongue mode strongly has changed. The variability in the eastern Atlantic is strongly reduced and the largest variability is now in the Benguela region. The explained variance is decreased form 14 % to 12 %. The seasonal cycle (Fig. 13c) is also reduced and no longer shows a strong maximum in boreal summer as in the CONTROL run and in the observations. A spectral analysis did not reveal a dominant spectral peak in the CONTROL as well as in the NO-MOC simulation. Observations hint at a period of about two years but this is not firmly established (Xie and Carton 2004).

The cold tongue mode is, similar as the El-Niño mode, the result of a "Bjerknes-Feedback". This feedback consists of three elements: the coupling between 1) SST and zonal wind stress, 2) zonal wind stress and ocean dynamics, and 3) ocean dynamics and SST. To understand the changes of the cold tongue mode we have analyzed the changes of these three elements of the "Bjerknes-Feedback".

This analysis is similar as done by Keenlyside and Latif (2007) for the observations. This enables us to compare the "Bjerknes-Feedback" in the model with the observations and to understand the causes for the changes in the cold tongue mode due to the collapse of the MOC. The results are shown in Fig. 14. Figures 14ab show that the response of the zonal wind stress in the western Atlantic to SST anomalies in the cold tongue region has been hardly changed and is similar as observed (Figure 1a in Keenlyside and Latif). Further analysis revealed that the almost similar response is the result of two counteracting effects. The warming in the cold tongue region in the NO-MOC experiment results in a larger response in rainfall and omega at 500 hPa (ω500) to SST anomalies. On the other hand, this warming reduces the east-west SST gradient over the Atlantic. This diminishes the zonal wind stress response in the western tropical Atlantic to ω500 anomalies over the cold tongue region. Figures 14cd shows a moderate reduction in the response of the ocean heat content to wind stress variations in the western Atlantic. Here we have, following Keenlyside and Latif (2007), taken sea level height (SLH) anomalies as a proxy for ocean heat anomalies. The collapse of the basin-wide MOC in the NO-MOC experiment results in a deepening of the thermocline. This deepening diminishes the thermocline response to wind stress variations. Finally Figs. 14de show that the response of SST to heat content anomalies in the cold tongue region has been strongly reduced. The deepening of the thermocline causes that thermocline depth variations no longer induce significant temperature changes in the mixed layer. The reduction of SST variability is largest in boreal summer in agreement with largest reduction of the entrainment in this season. The response of SST to heat content anomalies is hardly changed over the Benguela region, explaining that the cold tongue mode has its largest variability over the Benguela region in the NO-MOC experiment. In addition there is a positive feedback in the Benguela region with respect to the solar radiation, due to the reduction of stratus clouds with rising temperatures (not shown).

Comparing the three elements of the "Bjerknes-Feedback" in the CONTROL with the observations as computed by Keenlyside and Latif (2007) (Their Fig.1), it appears that the mechanism

of the cold tongue mode is simulated realistically in the CONTROL run. The main deviation is the large negative response in heat content in the south western tropical Atlantic to wind stress variation in the western tropical Atlantic (Fig.14c). We speculate that this is related to the too southern position of the ITCZ in the model.

3.3.2 Gradient mode

The gradient mode is forced by variations in the north-east trade winds (Czaja et al. 2002; Breugem et al. 2007a). Figures 13bd show that this mode of variability remains practically unaltered. The changes in the Hadley and extra-tropical circulation over the Atlantic are apparently too small to have a significant impact on the variability of the north-easterly trade winds in the region of the gradient mode. The reduction in the standard deviation of the SST close to the African coast, as seen in Fig. 12b, is caused by a decrease in the variability of the vertical entrainment due to a deepening of the mixed layer (Fig. 10). This has, however, no impact on the dynamics of the gradient mode which is forced by atmospheric fluxes.

4. Conclusions and discussion

Using Speedy-MICOM we have investigated the impact of the MOC on tropical Atlantic climate and variability. We have done this by analyzing the differences between a CONTROL run forced with Levitus et al. (1998) data at the northern and southern boundary of MICOM and a NO-MOC run in which these boundaries were replaced by ones that resulted in a collapse of the MOC. The SST response is characterized by a north-south SST dipole, with cooling in the North Atlantic and warming

in the tropical and South Atlantic, similar as obtained by for instance by Vellinga and Wood (2002), Dahl et al. (2005), Zhang and Delworth (2005), and Stouffer et al. (2006). A heat budget analysis revealed that for the tropical Atlantic the warming is mainly due to a reduction of the vertical entrainment of cold water in the mixed layer. Due to the collapse of the MOC the relatively cold South Atlantic no longer ventilates in the equatorial mixed layer. Instead the circulation is now dominated by the two STCs, resulting in a deepening of the thermocline. This causes a reduction of entrainment of cold water into the mixed layer and a warming of the equatorial Atlantic. The cooling in the North Atlantic mainly results from a reduction of the northward heat transport due to the weakening of the Gulf Stream and the North Atlantic drift.

The warming in the eastern tropical Atlantic is largest at the end of the boreal summer when the mixed layer depth is minimal due to the west African monsoon. The decrease in the cooling due to the reduction of the vertical entrainment has then the largest impact on the mixed layer temperature. This reduces the seasonal cycle in the eastern cold tongue region. The warming of the tropical Atlantic enhances the Hadley circulation, which is most prominent during the boreal summer.

The warming in the eastern tropical Atlantic and the reduction in the seasonal cycle also affect the interannual variability. The structure of the cold tongue mode is strongly modified and now resembles more a Benguela mode with its largest loading close to the coast of Angola. An analysis of the different elements of the "Bjerkenes-Feedback" revealed that the change in the cold tongue mode is mainly due to the fact that, as a result of the deepening of the thermocline, in the eastern tropical Atlantic thermocline variations no longer significantly affect the mixed layer temperatures. The gradient mode, which is forced by changes in the trade winds, remains largely unaffected in the NO-MOC run.

The dipole response in SST with a cooling in the North Atlantic and a warming in the tropical and South Atlantic is in agreement with previous modeling studies and paleo-records. Our analysis indicates that this response is ocean driven with changes in horizontal transport responsible for the

North Atlantic cooling and changes in vertical transport responsible for the tropical Atlantic warming.

Acknowledgments. This research was supported by FAPESP. This enabled Reindert Haarsma a 3 month visit at the oceanographic institute of the university of Sao Paulo (IOUSP) (Gant 2005/04315-0) and Edmo Campos (Grant 2006/03949-8) a 2 month visit at the KNMI in the Netherlands. The comments of two anonymous reviewers have significantly improved the manuscript.

References

Bleck, R., C. Rooth, D. Hu and L.T. Smith, 1992: Salinity-driven thermocline transients in a wind- and thermohaline-forced isopycnic coordinate model of the North Atlantic. *J. Phys. Oceanogr.,* **22,** 1486-1505.

Breugem, W.P., W. Hazeleger and R.J. Haarsma, 2007a: Mechanisms of northern tropical Atlantic variability and response to CO2 doubling. *J. Climate*, **20,** 2691-2705. doi:10.1175/JCLI4137.1

Breugem, W.P., W. Hazeleger and R.J. Haarsma, 2007b: Multimodel study of tropical Atlantic variability and change. *Geophys. Res. Lett.,* **33,** L23706 doi:10.1029/2006GL027831

Carton, J.A. and B. Huang, 1994: Warm events in the tropical Atlantic. *J. Phys. Oceanogr.,* **24,** 888-903.

Chang, P., L. Ji and H. Li, 1997: A decadal climate variation in the tropical Atlantic ocean from thermodynamic air-sea interactions. Nature, **385,** 516-518.

Czaja, A., P. van der Vaart and J. Marshall, 2002: A diagnostic study of the role of remote forcing in tropical Atlantic variability. *J. Climate,* **15,** 3280-3290.

Dahl, K.A., A.J. Broccoli and R. Stouffer, 2005: Assessing the role of North Atlantic freshwater forcing in millennial scale climate variability: A tropical Atlantic perspective. *Climate Dyn.,* **24,** 325-346.

Ganachaud, A. and C. Wunsch, 2003 Large scale ocean heat and freshwater transports during the World Ocean Circulation Experiment, *J. Climate,* **16,** 696-705.

Gregory, J. M. et al., 2005: A model intercomparison of changes in the Atlantic thermohaline circulation in response to increasing atmospheric CO_2 concentration. Geophys. Res. Lett., **32,** L12703.

Haarsma, R.J. en W. Hazeleger, 2007: Extra-tropical atmospheric response to equatorial Atlantic cold tongue anomalies. *J. Climate,* **20,** 2076-2091.

Hastenrath S., 1978: On modes of tropical circulation and climate anomalies. *J. Atmos. Sci.,* **35,** 2222-2231.

Hazeleger, W. and S. Drijfhout, 2006: Subtropical cells and meridional overturning circulation pathways in the tropical Atlantic. *J. Geophys. Res.,* **111,** doi:10.1029/2005JC002942.

Hazeleger, W, C. Severijns, R.J. Haarsma, F. Selten, A. Sterl, 2003: SPEEDO-model description and validation of a flexible coupled model for climate studies. KNMI, *Technical Report, TR-257, de Bilt, The Netherlands,* 37 pp.

Hazeleger, W. and R.J. Haarsma, 2005: Sensitivity of tropical Atlantic climate to mixing in a coupled ocean-atmosphere model. *Climate Dyn.,* **25,** 387-399, doi:10.1007/s00382-005-0047-y

Keenlyside, N. S and M. Latif, 2007: Understanding equatorial Atlantic interannual variability. *J Climate,* **20,** 131-142.

Large, W.G and S.G Yeager, 2004: Diurnal to decadal global forcing for ocean and sea-ice models: the data sets and flux climatologies, NCAR Technical Note: NCAR/TN-460+STR, CGD Division of the National Center for Atmospheric.

Lee, S. and H.-K. Kim, 2003: The dynamical relationship between subtropical and eddy-driven jets. *J. Atmos. Sci,* **60,** 1490-1503.

Levitus, S., T.P. Boyer, M.E. Conkright, T. O'Brien, J. Antonov, C. Stephens, L. Stathoplos, D. Johnson, R. Gelfeld, 1998: NOAA Atlas NESDIS 18, WORLD OCEAN DATABASE 1998: Vol 1: Introduction. US Government Printing Office, Washington DC, 346 pp.

Molteni, F., 2003: Atmospheric simulations using a GCM with simplified physical parameterizations. I: model climatology and variability in multi-decadal experiments. *Climate Dyn.,* **20,** 175-191.

Peterson, L.C., G.H. Haug, K.A. Hughen, U. Röhl, 2000: Rapid changes in the hydrological cycle of the tropical Atlantic during the last glacial. *Science*, **290,** 1947-1951.

Ruiz-Barradas A., J.A. Carton and S. Nigam., 2000: Structure of interannual-to-decadal climate variability in the Tropical Atlantic Sector. *J. Climate,* **13,** 3285-3297.

Son, S.-W. and S. Lee, 2005: The response of westerly jets to thermal driving in a primitive equation model. *J. Atmos. Sci.,* **62,** 3741–3757, doi: 10.1175/JAS3571.1

Stott, L., C. Poulsen, S. Lund and R. Thunell, 2002: Super ENSO and global climate oscillations at millennial time scales. *Science,* **297,** 222-226.

Stouffer et al., 2006: Investigating the causes of the response of the thermohaline circulation to past and future climate changes. *J. Climate,* **19,** 1365-1387.

Trenberth, K. E., and J. M. Caron, 2001: Estimates of meridional atmosphere and ocean heat transports. *J. Climate.,* **14,** 3433-3443.

Vellinga, M. and R.A. Wood, 2002: Global climatic impacts of a collapse of the Atlantic thermohaline circulation. *Climate Change,* **54,** 251-267.

Weijer, W, W. P. M. de Ruijter, H. A. Dijkstra and P. J. van Leeuwen, 1999: Impact of interbasin

exchange on the Atlantic overturning circulation. *J. Phys. Oceanogr.*, **29,** 2266-2284.

Xie, S.-P., 1999: A dynamic ocean-atmosphere model of tropical Atlantic decadal variability. *J. Climate,* **12,** 64-70.

Xie S.-P. and J. A. Carton, 2004: Tropical Atlantic variability: Patterns, Mechanisms and Impacts. In: *Earth Climate: The Ocean-Atmosphere Interaction.* C. Wang, S.-P. Xie and J.A. Carton (eds). Geophysical Monograph, AGU, Washington. D.C.

Yang, H. and Z. Liu, 2005: Tropical-extratropical climate interaction as revealed in idealized coupled climate model experiments. *Cimate Dyn.,* **24,** 863-879.

Zebiak, S.E., 1993: Air-sea interaction in the equatorial Atlantic region. *J. Climate,* **6,** 1567-1586.

Zhang, R., and T. L. Delworth, 2005: Simulated tropical response to a substantial weakening of the Atlantic thermohaline circulation. *J. Climate,* **18,** 1853-1860.

Figure Captions

Fig.1. (a) First REOF of monthly mean anomalous SST in ^{o}C (shaded) and the associated wind stress in Nm^{-2} (vectors) obtained by linear regression on the principal component normalized by its standard deviation. Dashed contours indicate negative SST values, the zero contour is omitted. (b) As (a) but now for the second REOF. The explained variances by the first and second REOF are 14 % and 10 % respectively.

Fig. 2. (a) Zonal mean temperature (^{o}C) profiles of the lateral boundaries in MICOM. Solid lines CONTROL run, dashed lines NO-MOC run. Thin lines northern boundary, thick lines southern boundary. (b) As (a) but now for salinity (PSU). (c) Zonally mean averaged difference in density (σ_θ) between the northern and southern boundary for the CONTROL run (solid) and the NO-MOC run (dashed).

Fig 3. (a) Annual mean difference in SST in ^{0}C (shaded) and wind stress in N m^{-2} (vectors) between the NO-MOC and CONTROL run. (b) Annual difference in SSS in PSU between the NO-MOC and CONTROL run. Dashed contours indicate negative values, the zero contour is omitted.

Fig. 4. (a) Omega in hPa s^{-1} averaged over (50^{o}W – 25^{o}E) for DJF. Thick contour lines: CONTROL run. Dashed lines indicate negative values (upward motion), the zero contour is omitted; Shaded: Difference between NO-MOC and CONTROL run. (b) As (a) but for JJA.

Fig. 5. (a) Rain fall in mm day^{-1} for DJF. Shaded: Difference between NO-MOC and CONTROL run. Dashed contours indicate negative values, the zero contour is omitted. The thick line indicates the 7.5 mm day^{-1} contour line in the CONTROL run. (b) As (a) but for JJA.

Fig. 6. Difference in zonal wind at 200 hPa in m s^{-1} between the NO-MOC and CONTROL experiment for DJF. Dashed contours indicate negative values, the zero contour is omitted.

Fig. 7. Changes in the annual mean heat budget of the mixed layer between the NO-MOC and CONTROL run: (a) net surface heat flux in Wm^{-2} (downward is positive). (b) vertical ocean heat transport in K s^{-1}.

Fig. 8. (a) Meridional overturning circulation in Sv for the CONTROL run. (b) As (a) but for the NO-MOC run. (c) Meridional heat transport in PW for the CONTROL (solid line) and NO-MOC experiment (dashed line).

Fig. 9. Cross-section along the equator of the temperature difference (^{o}C) between the CONTROL and NO-MOC run. Dashed contours indicate negative values, the zero contour is omitted. The thick solid and dashed lines indicate the depth of the 20 ^{o}C isotherm for the CONTROL and NO-MOC run respectively.

Fig. 10. Relative change in the annual mean mixed layer depth (%) between the NO-MOC and CONTROL run.

Fig. 11. (a) Seasonal cycle of the vertical entrainment (10^{-6} K s^{-1}) along the equator for the CONTROL run (contours) and for the difference between NO-MOC and CONTROL run (shaded). (b) As (a) but for the SST (^{o}C).

Fig. 12. Standard deviation of monthly mean anomalous SST in ^{o}C for the CONTROL run (a) and the

NO-MOC run (b).

Fig. 13. (a) For the NO-MOC run the first REOF of monthly mean anomalous SST in ^{o}C and the associated wind stress in N m^{-2} (vectors) obtained by linear regression on the principal component normalized by its standard deviation. (b) As (a) but now for the second REOF. (c) Seasonal cycle of the first principal component of the first REOF for the NO-MOC run (solid) and CONTROL run (dashed). (d) As (c), but for the second REOF. The explained variances by the first and second REOF are 12 % and 11 % respectively.

Fig. 14. (a and b) Regression between monthly mean SST anomalies (ºC) averaged over 3ºS-3ºN, 10ºW-10ºE (black box) and zonal wind stress anomalies (Nm^{-2}) for the CONTROL and NO-MOC run. The regression is multiplied by 10^3. (c and d) Regression between monthly mean zonal wind stress anomalies averaged over (3ºS-3ºN, 40ºW-20ºW) (black box) and SSH anomalies (m) for the CONTROL and NO-MOC run. (e and f) Regression at every grid point between monthly mean SSH anomalies and SST anomalies.

a b

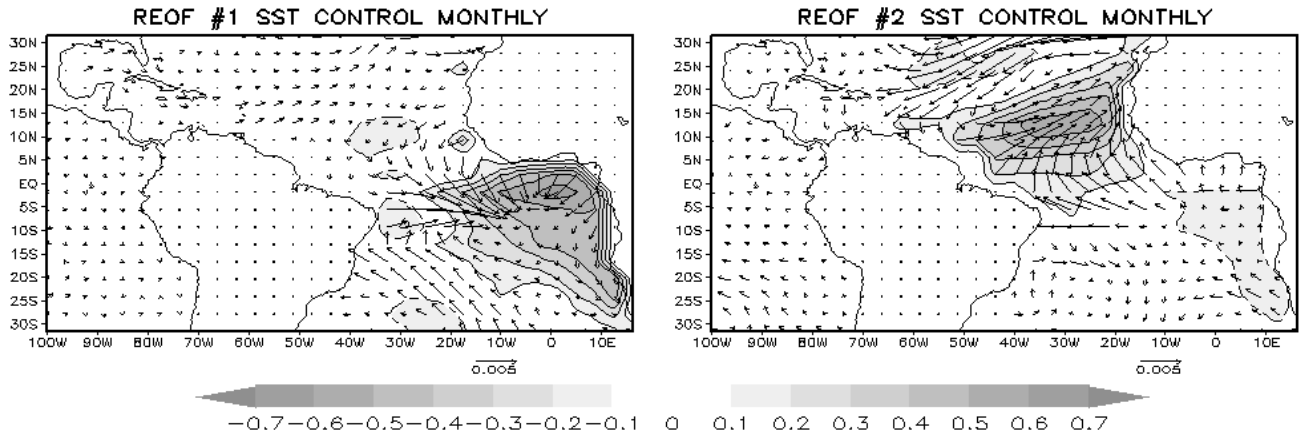

Fig.1. (a) First REOF of monthly mean SST in ^{o}C (shaded) and the associated wind stress in Nm^{-2} (vectors) obtained by linear regression on the principal component normalized by its standard deviation. Dashed contours indicate negative SST values, the zero contour is omitted. (b) As (a) but now for the second REOF. The explained variances by the first and second REOF are 14 % and 10 % respectively.

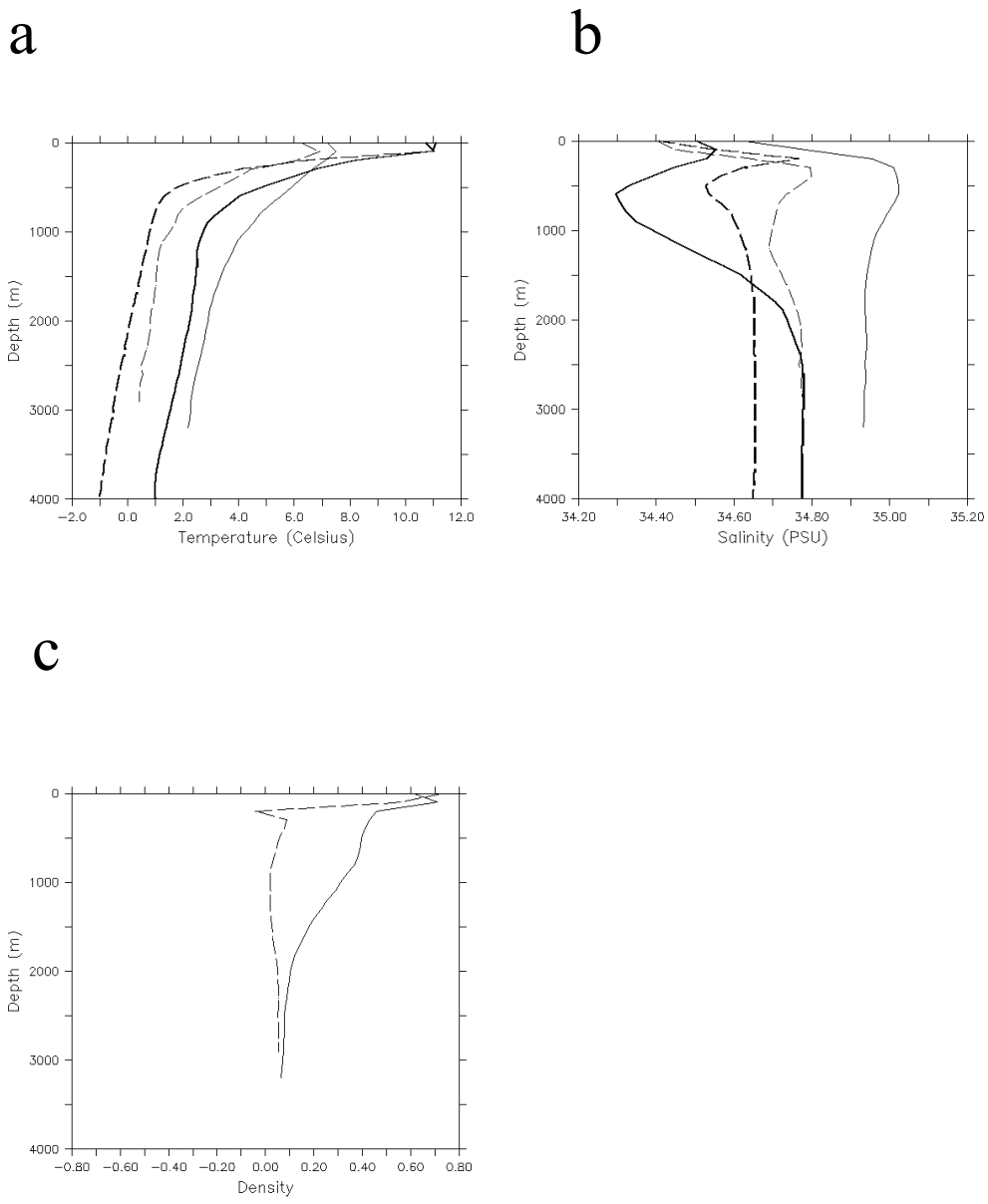

Fig. 2. (a) Zonal mean temperature (^{o}C) profiles of the lateral boundaries in MICOM. Solid lines CONTROL run, dashed lines NO-MOC run. Thin lines northern boundary, thick lines southern boundary. (b) As (a) but now for salinity (PSU). (c) Zonally mean averaged difference in density (σ_θ) between the northern and southern boundary for the CONTROL run (solid) and the NO-MOC run (dashed).

Fig. 3a

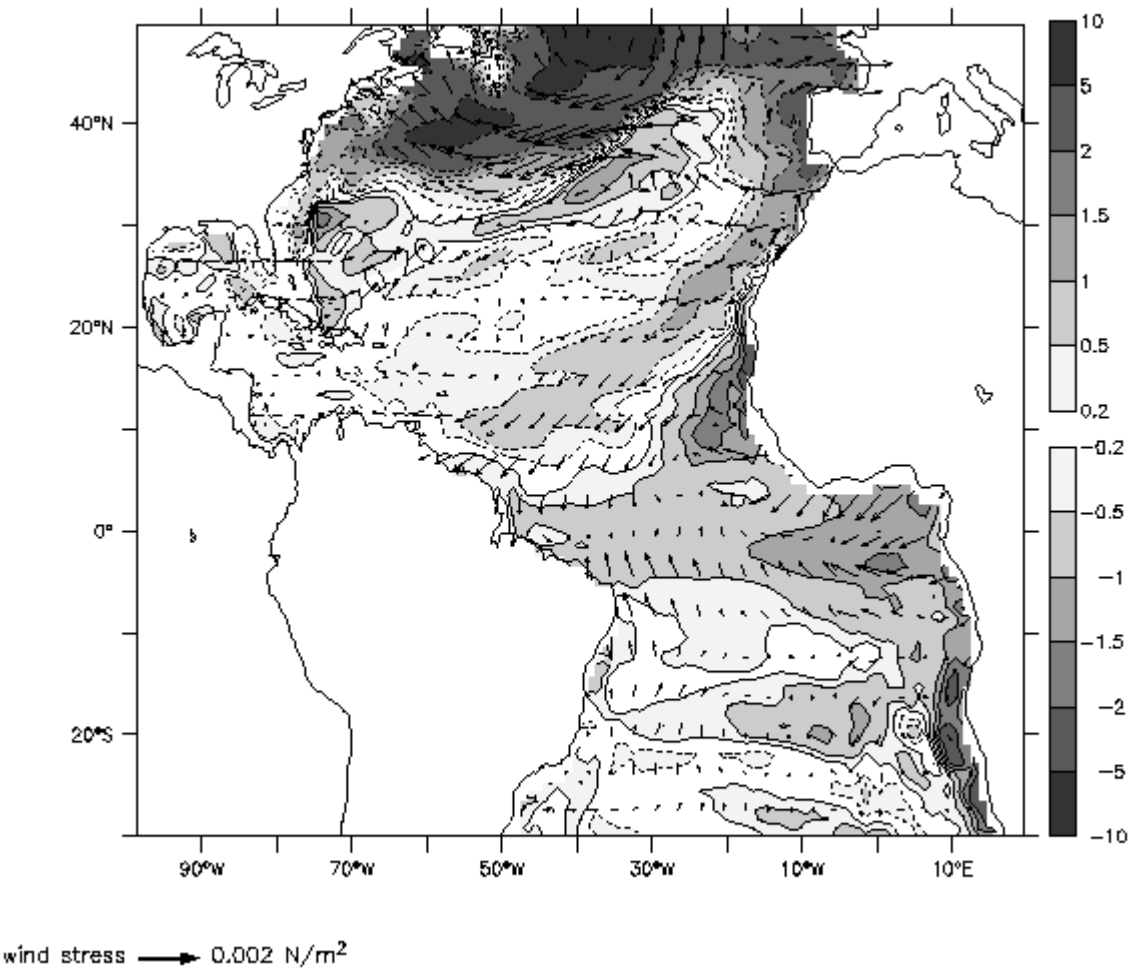
40°N
20°N
0°
20°S
90°W
70°W
50°W
30°W
10°W
10°E
10
5
2
1.5
1
0.5
0.2
−0.2
−0.5
−1
−1.5
−2
−5
−10
wind stress 0.002 N/m²

Fig. 3b

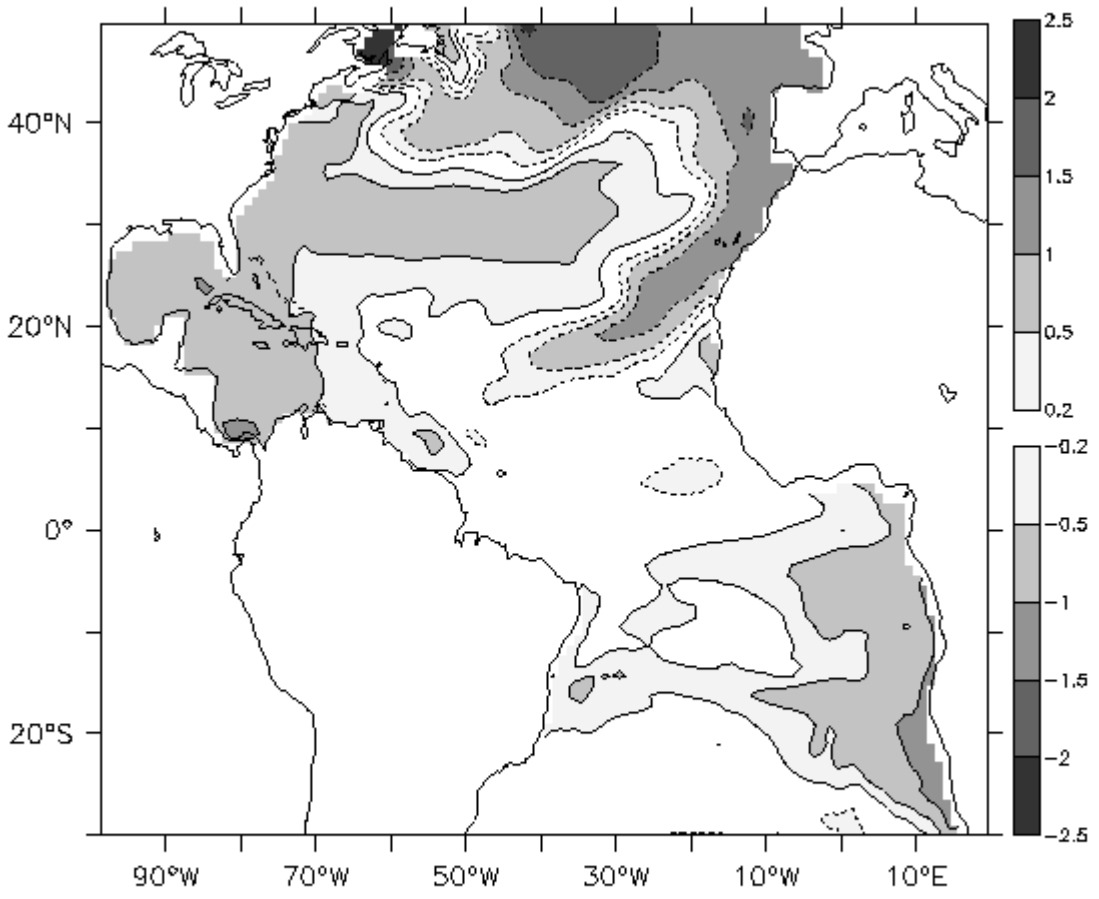

Fig 3. (a) Annual mean difference in SST in ^{0}C (shaded) and wind stress in N m^{-2} (vectors) between the NO-MOC and CONTROL run. (b) Annual difference in SSS in PSU between the NO-MOC and CONTROL run. Dashed contours indicate negative values, the zero contour is omitted.

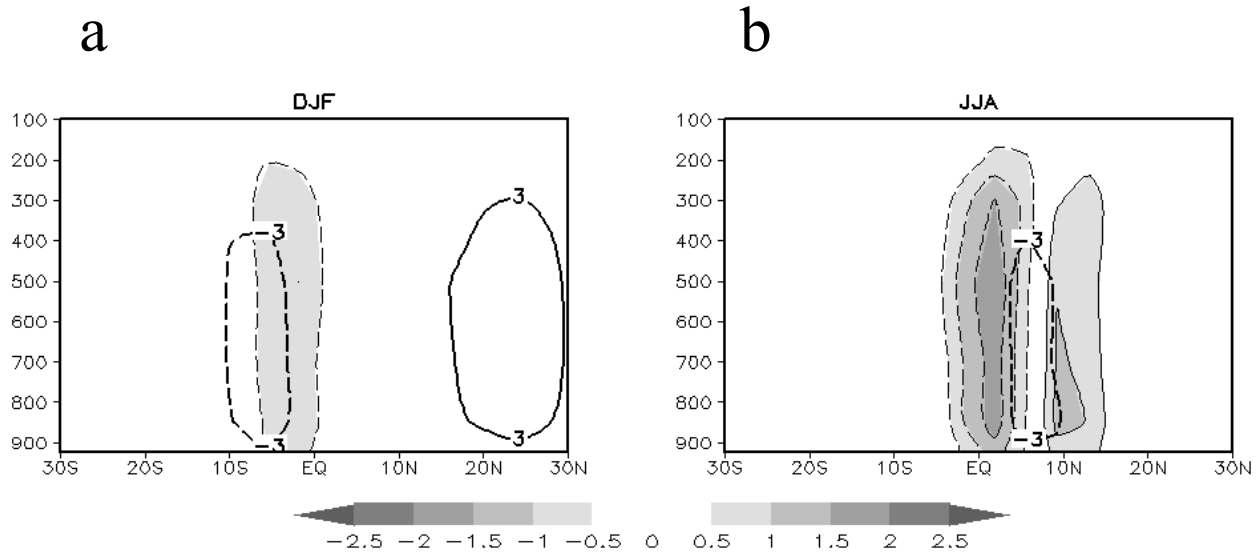

Fig. 4. (a) Omega in hPa s^{-1} averaged over (50°W – 25°E) for DJF. Thick contour lines: CONTROL run. Dashed lines indicate negative values (upward motion), the zero contour is omitted; Shaded: Difference between NO-MOC and CONTROL run. (b) As (a) but for JJA.

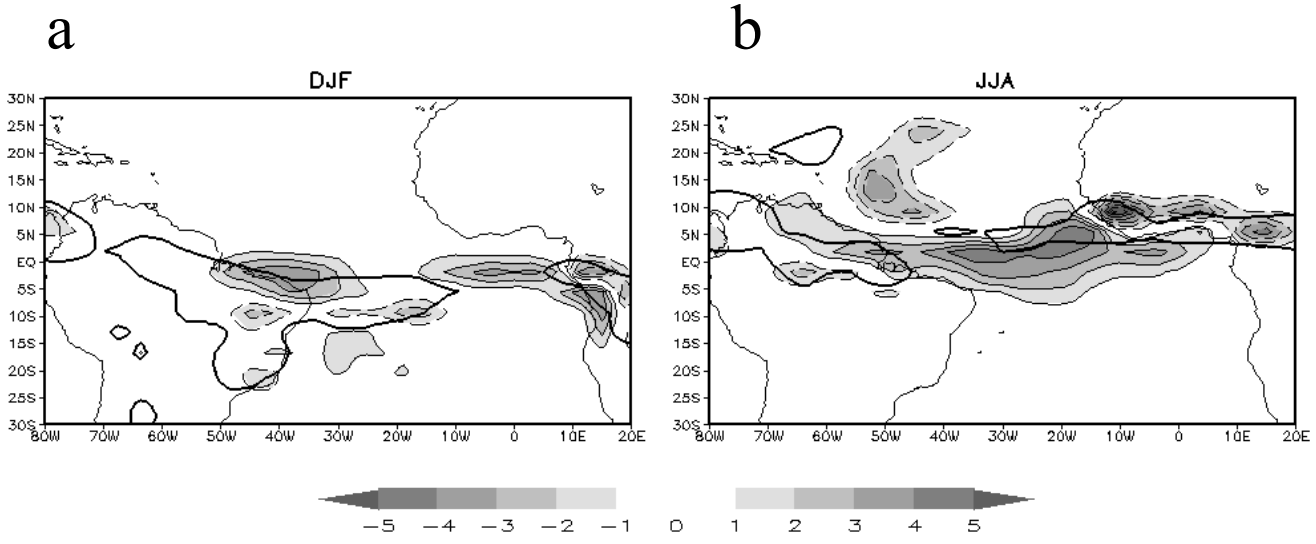

Fig. 5. (a) Rain fall in mm day^{-1} for DJF. Shaded: Difference between NO-MOC and CONTROL run. Dashed contours indicate negative values, the zero contour is omitted. The thick line indicates the 7.5 mm day^{-1} contour line in the CONTROL run. (b) As (a) but for JJA.

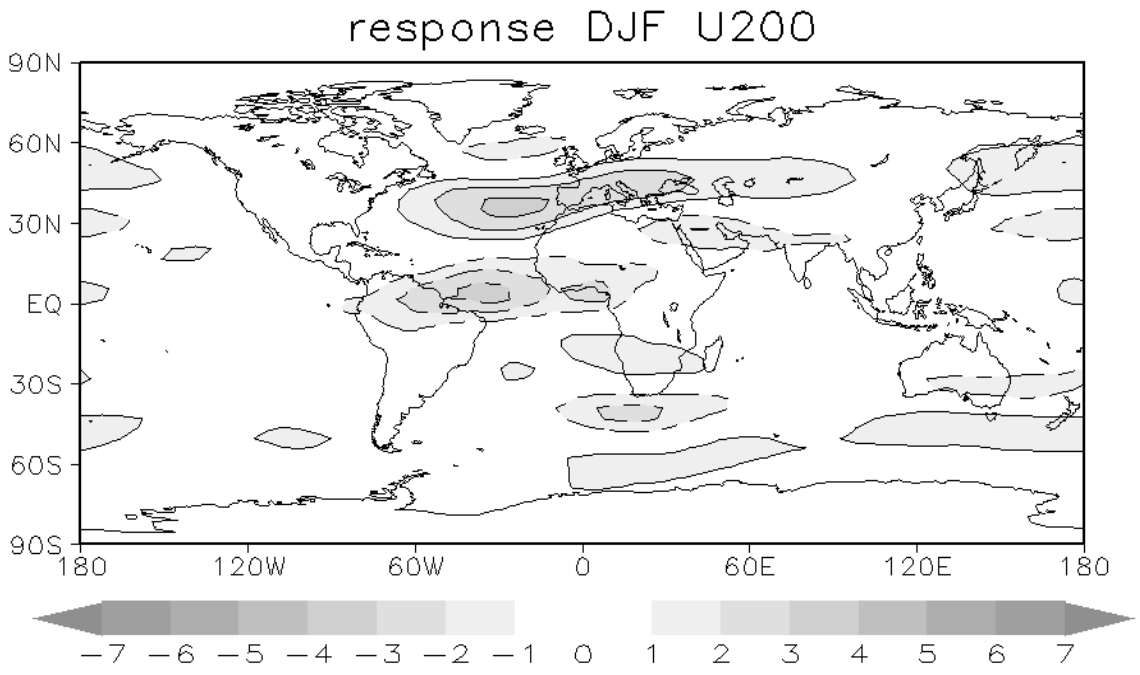

Fig. 6. Difference in zonal wind at 200 hPa in m s^{-1} between the NO-MOC and CONTROL experiment for DJF. Dashed contours indicate negative values, the zero contour is omitted.

Fig. 7a

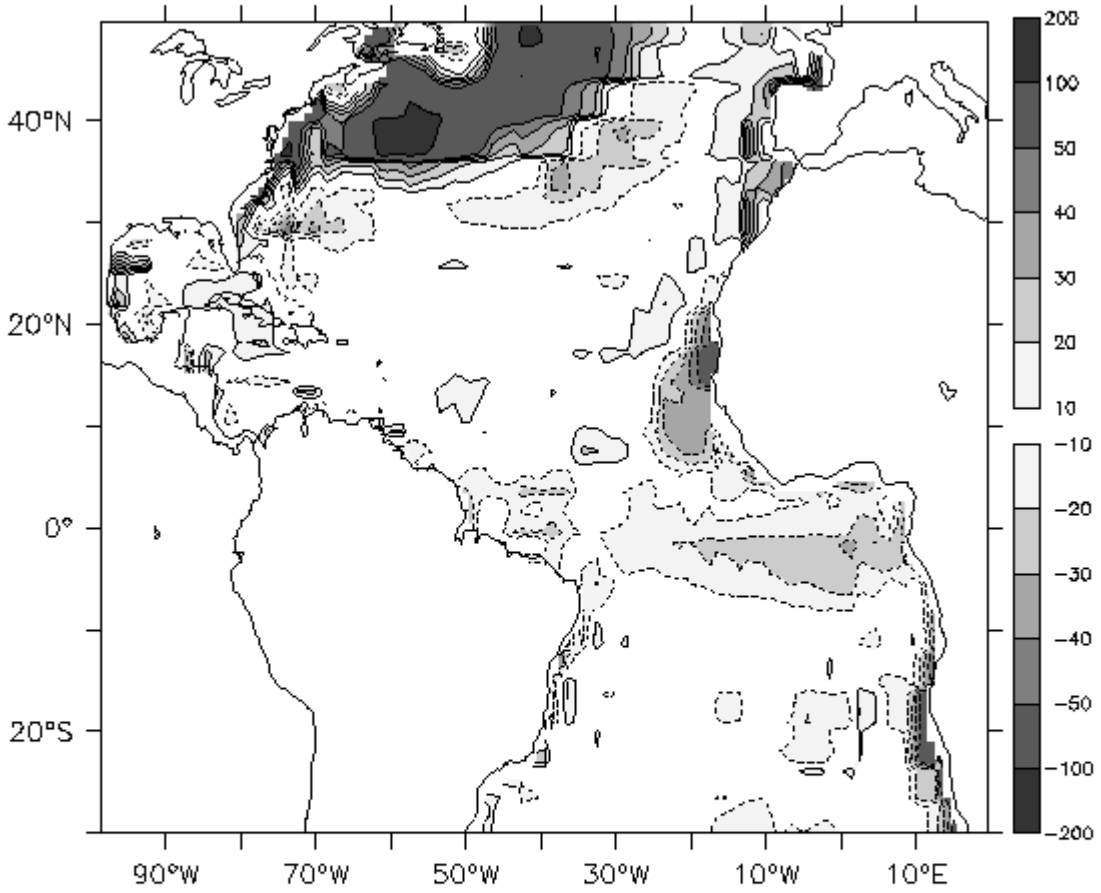
40°N
20°N
0°
20°S
90°W
70°W
50°W
30°W
10°W
10°E
200
100
50
40
30
20
10
−10
−20
−30
−40
−50
−100
−200

Fig. 7b

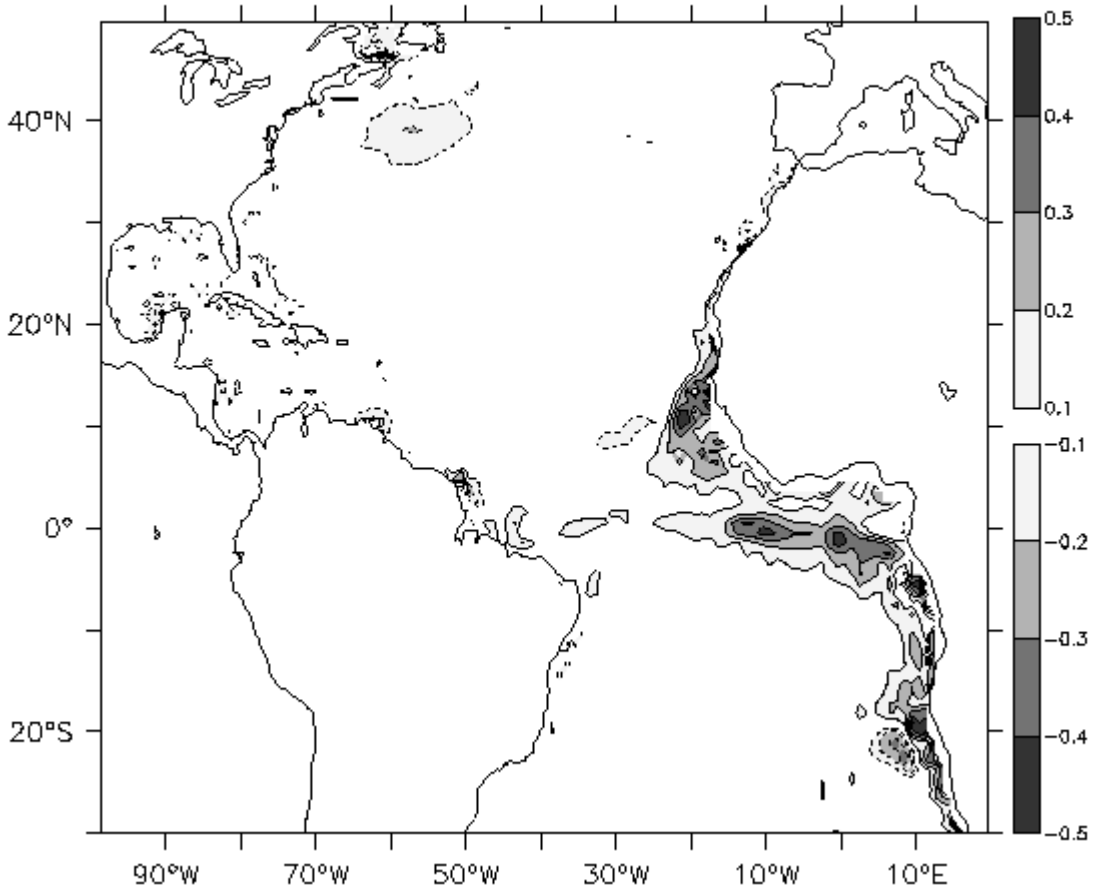

Fig. 7. Changes in the annual mean heat budget of the mixed layer between the NO-MOC and CONTROL run: (a) net surface heat flux in Wm^{-2} (downward is positive). (b) vertical ocean heat transport in $K\ s^{-1}$

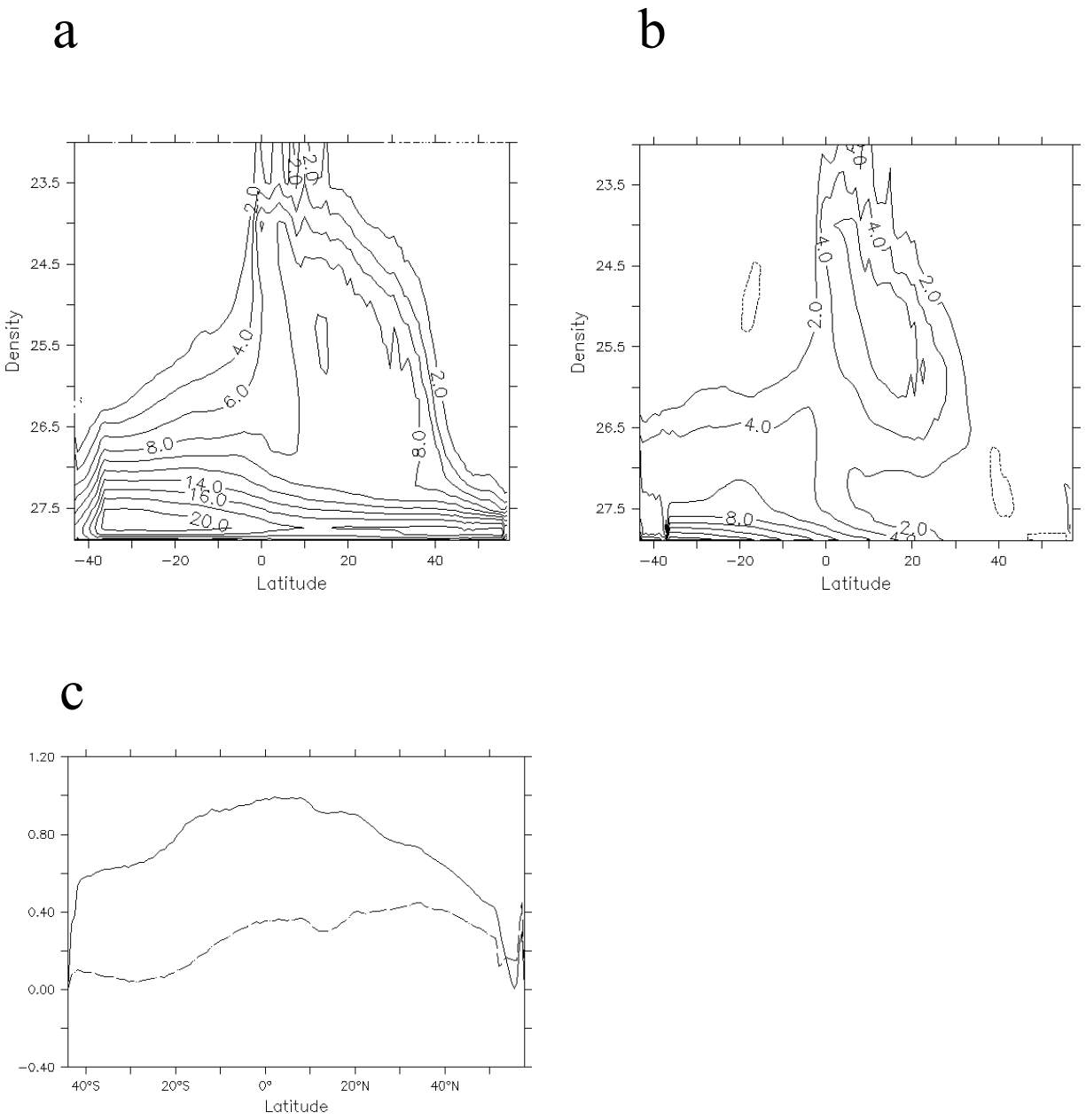

Fig. 8. (a) Meridional overturning circulation in Sv for the CONTROL run. (b) As (a) but for the NO-MOC run. (c) Meridional heat transport in PW for the CONTROL (solid line) and NO-MOC experiment (dashed line).

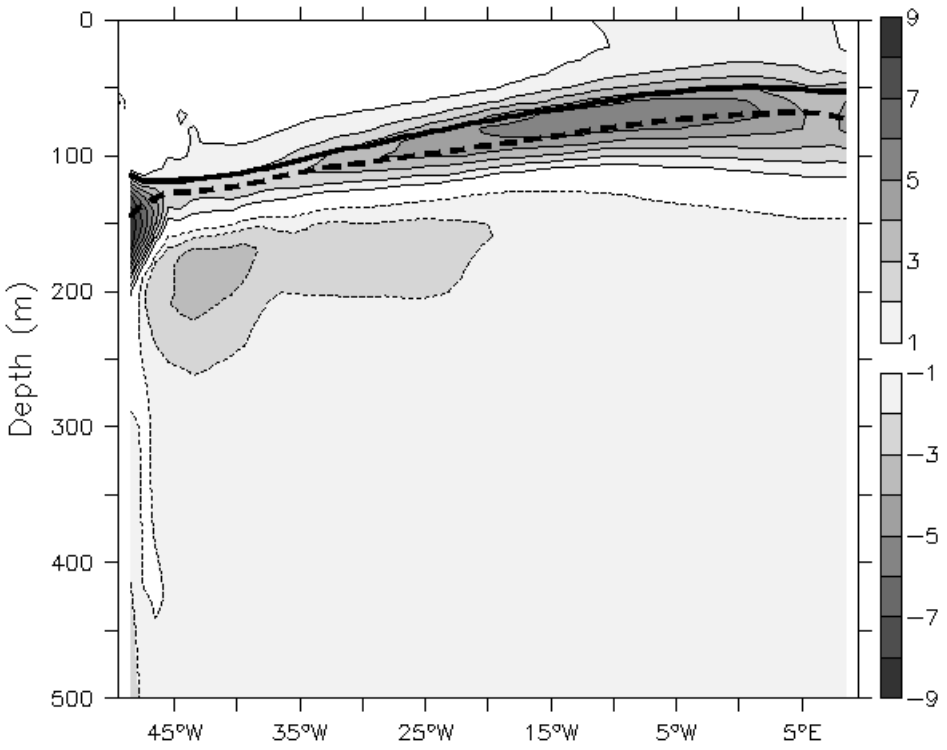

Fig. 9. Cross-section along the equator of the temperature difference (^{o}C) between the CONTROL and NO-MOC run. Dashed contours indicate negative values, the zero contour is omitted. The thick solid and dashed lines indicate the depth of the 20 ^{o}C isotherm for the CONTROL and NO-MOC run respectively.

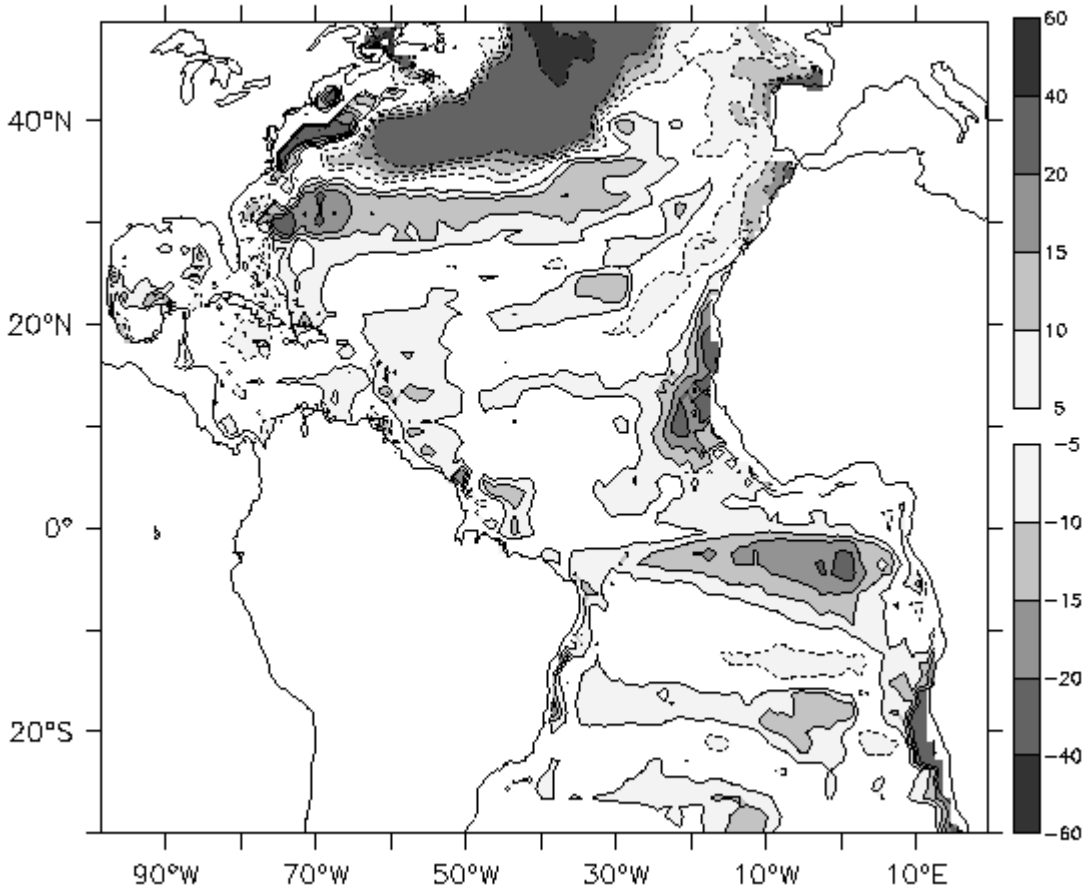

Fig. 10. Relative change in the annual mean mixed layer depth (%) between the NO-MOC and CONTROL run.

Fig 11a

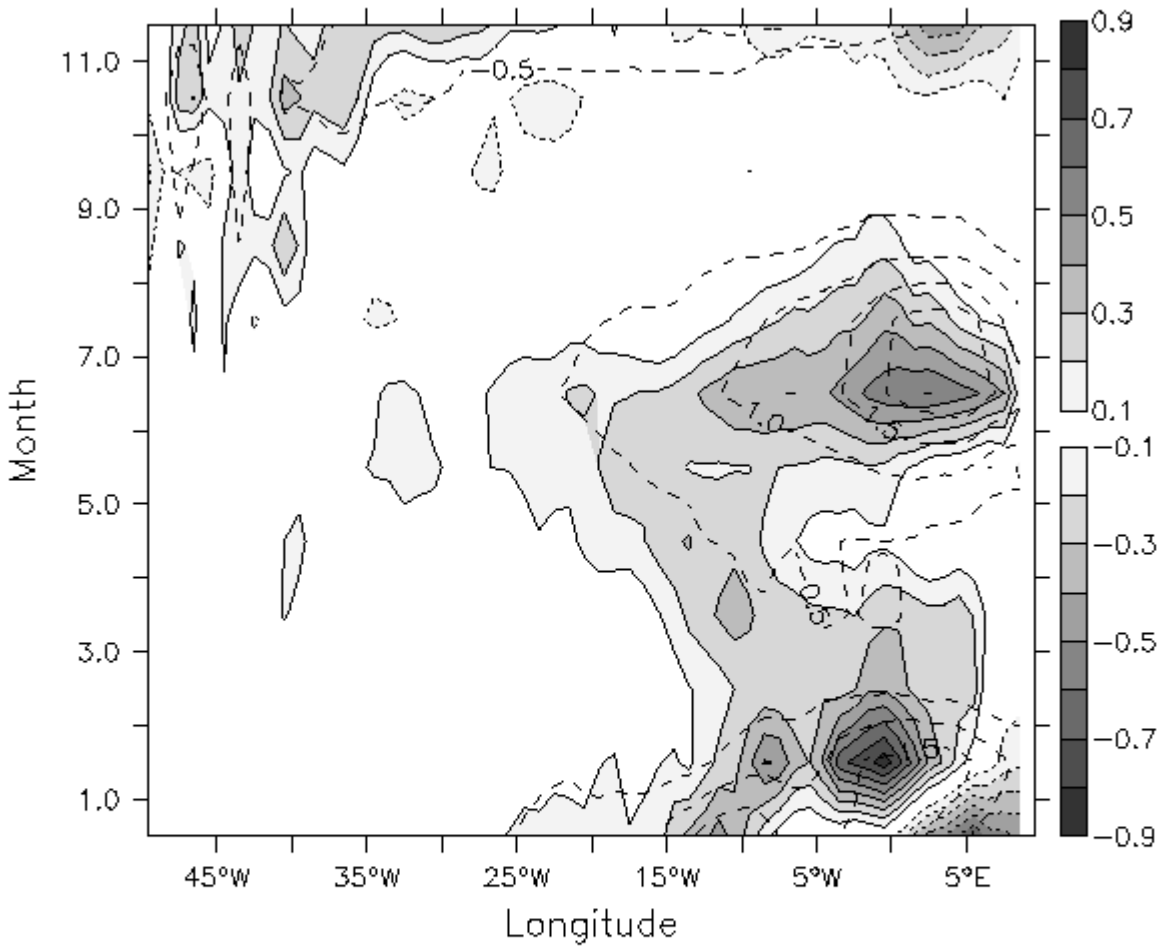
11.0
9.0
7.0
5.0
3.0
1.0
Month
45°W
35°W
25°W
15°W
5°W
5°E
Longitude
0.9
0.7
0.5
0.3
0.1
−0.1
−0.3
−0.5
−0.7
−0.9

Fig. 11b

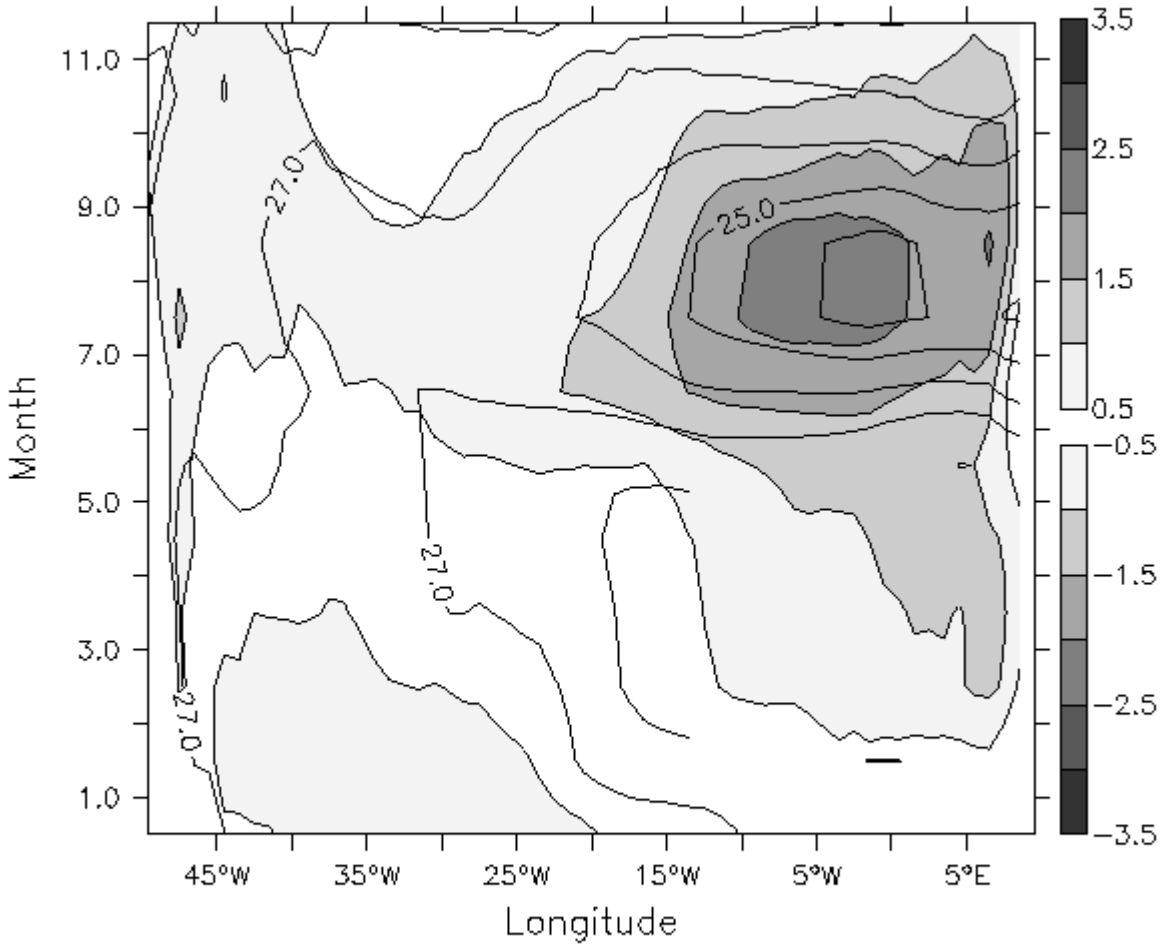

Fig. 11. (a) Seasonal cycle of the vertical entrainment (10^{-6} K s^{-1}) along the equator for the CONTROL run (contours) and for the difference between NO-MOC and CONTROL run (shaded). (b) As (a) but for the SST (^{o}C).

a b

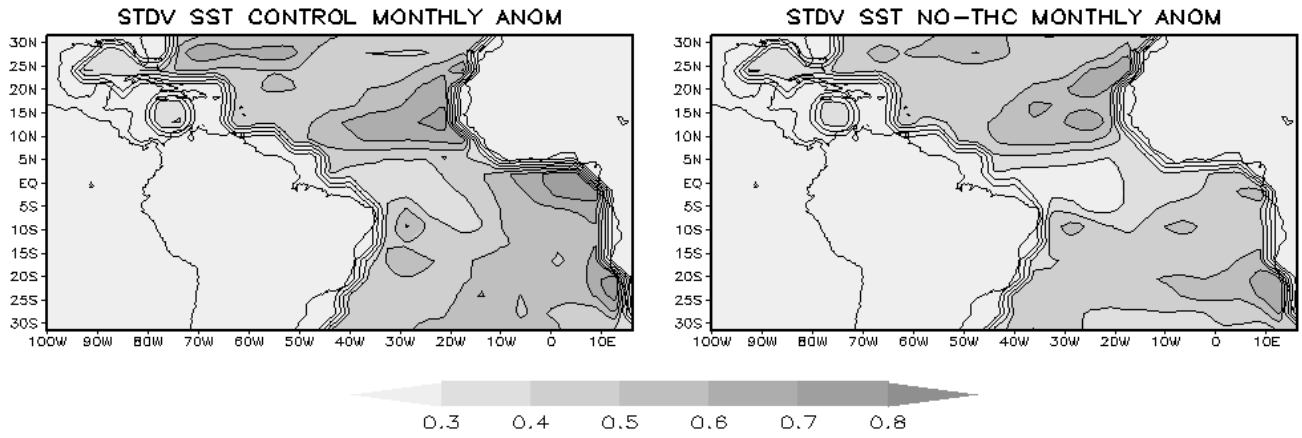

Fig. 12. Standard deviation of monthly mean anomalous SST in ^{o}C for the CONTROL run (a) and the NO-MOC run (b).

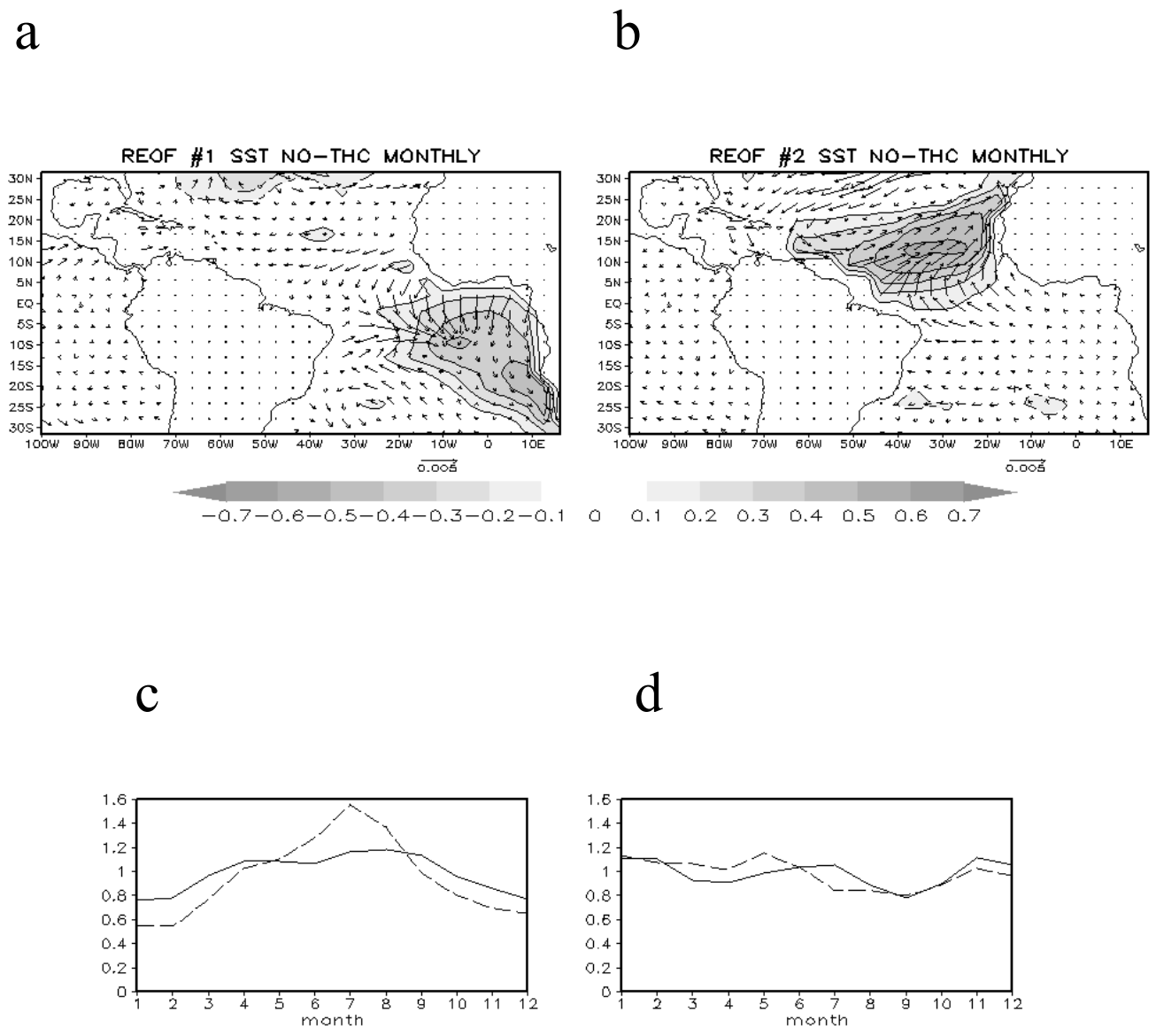

Fig. 13. (a) For the NO-MOC run the first REOF of monthly mean anomalous SST in ^{o}C and the associated wind stress in N m^{-2} (vectors) obtained by linear regression on the principal component normalized by its standard deviation. (b) As (a) but now for the second REOF. (c) Seasonal cycle of the first principal component of the first REOF for the NO-MOC run (solid) and CONTROL run (dashed). (d) As (c), but for the second REOF. The explained variances by the first and second REOF are 12 % and 11 % respectively.

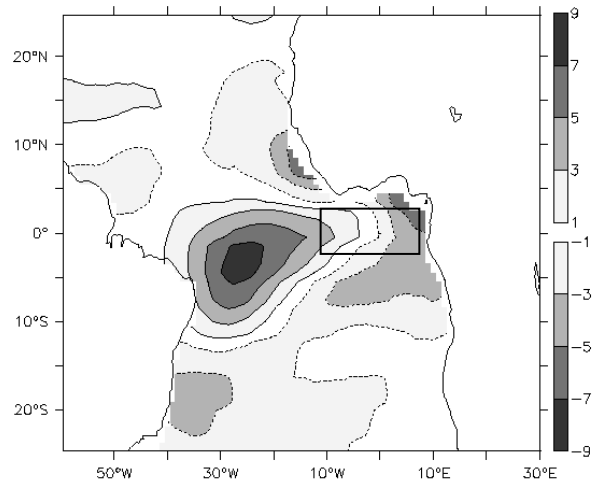
20°N
10°N
0°
10°S
20°S
50°W
30°W
10°W
10°E
30°E
9
7
5
3
1
−1
−3
−5
−7
−9

a

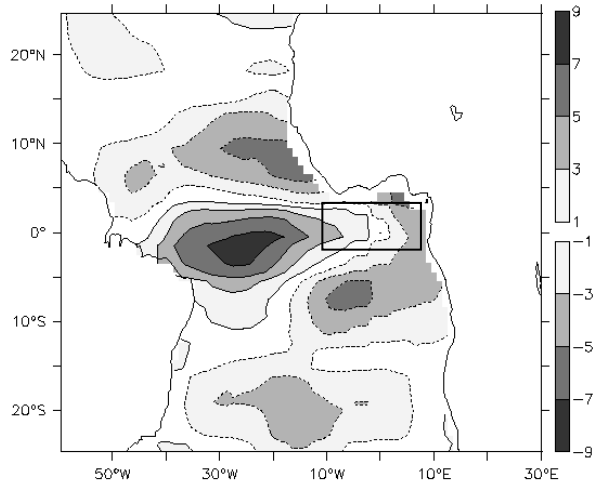
20°N
10°N
0°
10°S
20°S
50°W
30°W
10°W
10°E
30°E
9
7
5
3
1
−1
−3
−5
−7
−9

b

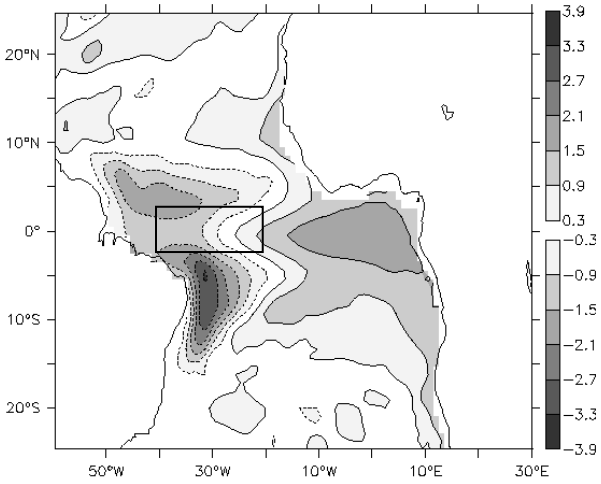
20°N
10°N
0°
10°S
20°S
50°W
30°W
10°W
10°E
30°E
3.9
3.3
2.7
2.1
1.5
0.9
0.3
−0.3
−0.9
−1.5
−2.1
−2.7
−3.3
−3.9

c

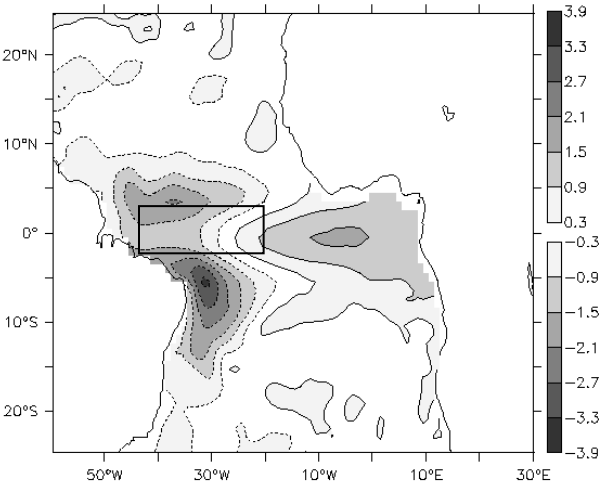
20°N
10°N
0°
10°S
20°S
50°W
30°W
10°W
10°E
30°E
3.9
3.3
2.7
2.1
1.5
0.9
0.3
−0.3
−0.9
−1.5
−2.1
−2.7
−3.3
−3.9

d

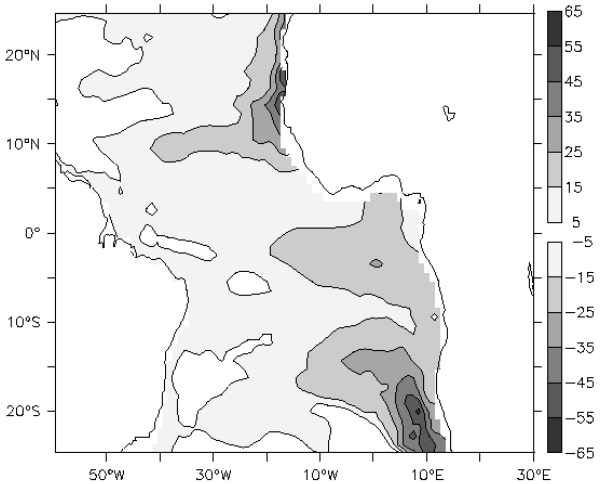
20°N
10°N
0°
10°S
20°S
50°W
30°W
10°W
10°E
30°E
65
55
45
35
25
15
5
−5
−15
−25
−35
−45
−55
−65

e

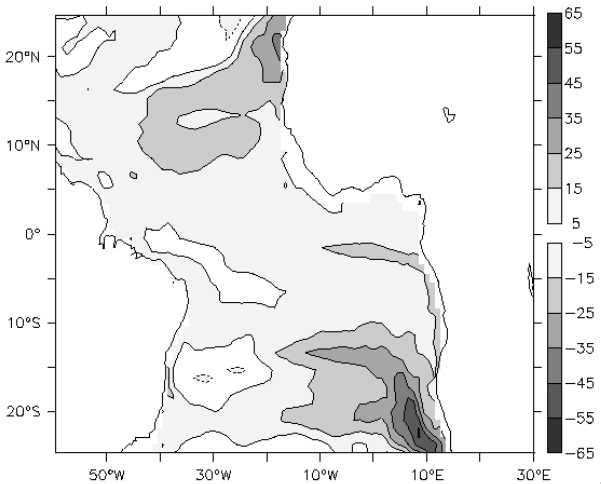
20°N
10°N
0°
10°S
20°S
50°W
30°W
10°W
10°E
30°E
65
55
45
35
25
15
5
−5
−15
−25
−35
−45
−55
−65

f

Fig. 14. (a and b) Regression between monthly mean SST anomalies (ºC) averaged over 3ºS-3ºN, 10ºW-10ºE (black box) and zonal wind stress anomalies (Nm^{-2}) for the CONTROL and NO-MOC run. The regression is multiplied by 10^3. (c and d) Regression between monthly mean zonal wind stress anomalies averaged over (3ºS-3ºN, 40ºW-20ºW) (black box) and SSH anomalies (m) for the CONTROL and NO-MOC run. (e and f) Regression at every grid point between monthly mean SSH anomalies and SST anomalies.